

Lamellar and inverse micellar structures of skin lipids: Effect of templating

Chinmay Das,^{1,*} Massimo G. Noro,^{2,†} and Peter D. Olmsted^{1,‡}

¹*School of Physics and Astronomy, University of Leeds, Leeds LS2 9JT, United Kingdom*

²*Unilever R&D, Port Sunlight, Wirral, CH63 3JW, United Kingdom*

(Dated: November 21, 2018)

The outermost layer of skin comprises rigid non-viable cells (corneocytes) in a layered lipid matrix. Using atomistic simulations we find that the equilibrium phase of the skin lipids is inverse micellar. A model of the corneocyte is used to demonstrate that lamellar layering is induced by the patterned corneocyte wall. The inverse micellar phase is consistent with *in vivo* observations in regions where corneocyte walls are well separated (lacunar spaces) and in the inner layers of skin, and suggests a functional role in the lipid synthesis pathway *in vivo*.

PACS numbers: 87.16.D- 87.10.Tf 61.30.Pq

Introduction: The outermost layer of skin, the stratum corneum (SC), comprises non-viable rigid cells (mainly keratin filled corneocytes) in a lipid matrix (Fig. 1a). The continuous lipid matrix is responsible for the extraordinary barrier property of skin and is the first line of defence against invasion of foreign pathogens [1]. The integrity of the lipid matrix is essential for proper functioning of skin, and an understanding of its structures will help in the design of agents to rejuvenate damaged lipid layers and selectively perturb the lipid structure to temporarily and reversibly increase the permeability for trans-dermal drug delivery [2].

The SC matrix is conspicuous by the absence of lipids with polar head groups and by having large molecular polydispersity. The earliest models introduced a coarse picture of “bricks” (corneocyte) surrounded by “mortar” (lipid) [3]. Later *in vivo* observations [4–7], and experiments with reconstituted SC lipid layers [8, 9], showed a multilamellar arrangement of lipids. Scattering experiments [5, 6, 9] and cryo-EM [4, 7] images yielded a large number of apparently contradictory results: lipids in gel-like [10] or fluid phases [11], one [7] or two [6] periodicities (in a multilayer arrangement), and signatures of different crystalline arrangements [12]. Existing models [13–18] have described some of these features by including specific lipids in particular positions of essentially a periodic crystalline arrangement. However, skin employs more than 300 different lipid molecules, and the relative concentrations of the different components vary widely (more than 100% between individuals and across the body sites of the same individual [19]) without affecting the normal skin function. A periodic fixed molecular arrangement is unlikely to accommodate such large variations in composition, or explain the low but finite permeability for small molecules [20], the pliability of healthy skin in accommodating deformation from mechanical and hydration stresses [21], or the activity of colocalised antimicrobial peptides and proteases [22].

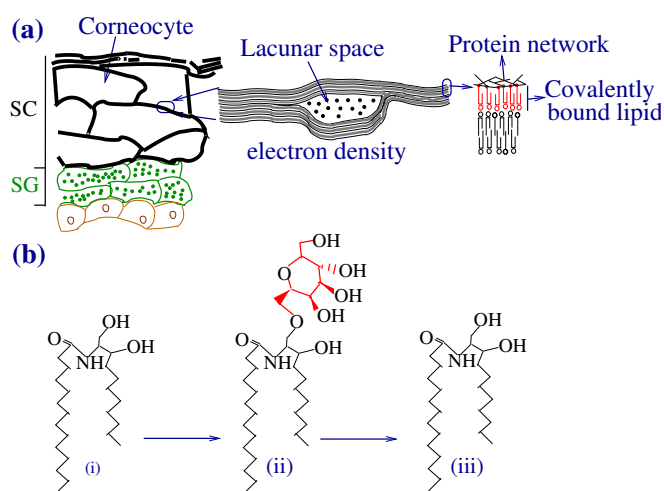


FIG. 1. (color online) (a) Schematic representation of the top two layers of skin: SC, the outermost layer, contains rigid corneocytes in a lipid matrix. Between corneocytes, the lipids show a periodic electron density pattern that is lost when the corneocyte walls are further apart [7]. A layer of lipids are covalently bound to the protein network of corneocytes forming the ‘corneocyte bound lipid envelope’ (CLE). (b) CER is synthesised in SG, the layer immediately below SC. After synthesis, a sugar moiety is added to the head group and the resulting galactoceramides are released by endocytosis. Enzymes remove the sugar group to revert back to CER in the intercellular space [23].

Ceramide sphingolipids (CER) constitute ~ 30 mol% of SC lipids [24, 25]. CER is synthesised in the stratum granulosum (SG), a layer below the SC [23]. Immediately after synthesis a sugar moiety is attached to the head group of the CER (fig. 1b) and the resulting galactoceramides are secreted by endocytosis. Enzymes in the extra-cellular space remove the sugar group to revert the molecules back to CER [23]. In response to removing the SC lipids by chemical insult, cells in the SG release lipid vesicles within minutes [26], but the permeability barrier recovers only after a few days [27]. The seemingly unnecessary step of attaching and removing a head group, and the large separation of time-scale between lipid release

* c.das@leeds.ac.uk

† Massimo.Noro@unilever.com

‡ p.d.olmsted@leeds.ac.uk

and barrier recovery, remain unexplained.

Previous molecular simulations of SC lipids have been limited to selected lipid components in pre-formed hydrated bilayers without realistic polydispersity [28–34]. Here we report results from large scale molecular dynamics simulations ($\sim 4 \times 10^6$ united atoms and μs time scales) of SC lipids with realistic polydispersity. The main findings are: (i) Randomly oriented initial conditions lead to an inverse-micellar arrangement in 30 wt% water. (ii) This structure is not just kinetically trapped, since an initial lamellar phase structure transforms to an inverted phase in simulation time-scales. (iii) A weak multilamellar arrangement develops when the lipid molecules are confined between two walls that mimic the corneocyte-bound lipid envelope. These results are consistent with existing *in-vivo* and *in-vitro* observations on the SC lipid arrangements, and can shed light on the relevance of the temporary addition of a head group in ceramide biosynthesis and the reason for separation of lipid-release and barrier-recovery timescales.

Simulations: The three main lipid components of the SC are CER, free fatty acids (FFA), and cholesterol (CHOL) [24, 25]. By changing the numbers and positions of the hydroxy groups in the sphingosine motif, nature uses 11 different families of CER molecules - each having large polydispersity in the tail lengths [35]. FFA molecules also show similar polydispersity in the tail lengths. We use the GROMACS molecular dynamics package [36] with the ‘Berger’ force-field [37, 38] for the lipids and the SPC model for the water molecules. To probe the bulk arrangement, for the 1:1:1 composition (molar ratio of CER, CHOL and FFA), we use 2000 CER, 2000 CHOL and 2000 FFA molecules and 50000 water molecules (3.7×10^6 united atoms). We use three members of the ceramide family (CER NS, CER NP and CER EOS Fig.2), with the experimentally observed tail length polydispersity, and thus 15 different CER molecules. The molar fractions of these three families were increased to account for the CER molecules of similar structure not explicitly considered in the simulations. Simulation details are included in the online supplementary material [35].

Hydrated bulk SC lipids - inverse micelles: To probe the bulk structure of the SC lipids in 30 wt.% water (approximate water content in the outer SC [39], though much of this water remains inside corneocytes [40]) with the least amount of bias, we place randomly oriented lipid and water molecules at random positions in a large simulation box. The imposed atmospheric pressure compresses this ‘gas’ until most of the water molecules aggregate into a few large and roughly spherical clusters, leading to an inverse-micellar phase (Fig. 3). We used three different initial conditions each for 1:1:1 and 2:2:1 composition ratios of CER, CHOL and FFA molecules. In all cases the system acquired an inverse micellar phase [35].

In one of the 2:2:1 systems we prepared the initial simulation box with the z -dimension much smaller than

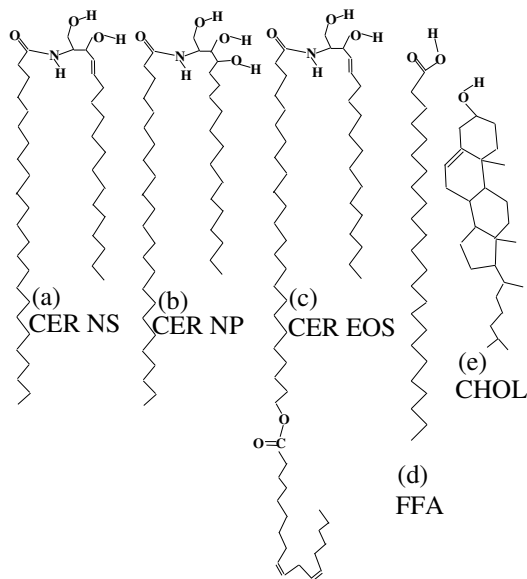


FIG. 2. Schematic representation of selected SC lipid molecules: CER NP (b) differs from CER NS (a) by having an extra OH group. CER EOS (c) contains an additional linoleic acid conjugated to the fatty acid tail. Both CER (a-c) and FFA (d) have large polydispersity in the tail lengths.

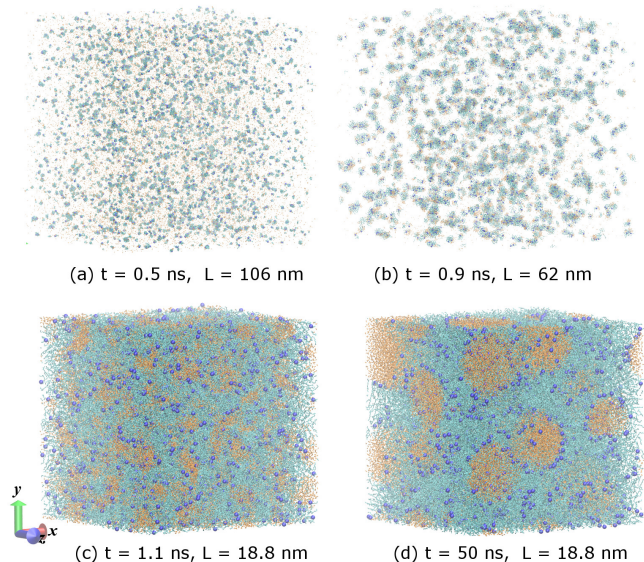


FIG. 3. Evolution of structure in 1:1:1 molar ratio of CER, CHOL and FFA SC lipids (cyan) with 30 wt.% water (orange). (a): 0.5 ns after random placement of the molecules in a box of dimension $L = 120\text{nm}$, L reduces slightly to 106nm. Water and lipid molecules start to cluster. (b): At 0.9 ns the clustering is more pronounced and the density increases quickly ($L \sim 62\text{nm}$). (c): At 1.1 ns the equilibrium density has been reached ($L \sim 18.8\text{nm}$). The clumping of water is now more pronounced. (d): By 50ns, the water molecules have arranged in a few large roughly spherical droplets, enclosed by coronae of lipid molecules [35].

the lateral dimensions. After the isotropic compression to atmospheric pressure, but before the water molecules formed isolated clusters, we used different imposed pressures along the z -direction (1 bar) and the lateral directions (1000 bar). The resulting flow aligns the lipid tails preferentially along the z -direction. Once the box becomes roughly cubic, we switched back to an isotropic pressure coupling. The final structure, once again, is an inverse micellar arrangement with the lipid tails isotropically distributed. This shows that liquid-crystalline ordering of the lipid molecules alone is not strong enough to sustain a lamellar arrangement.

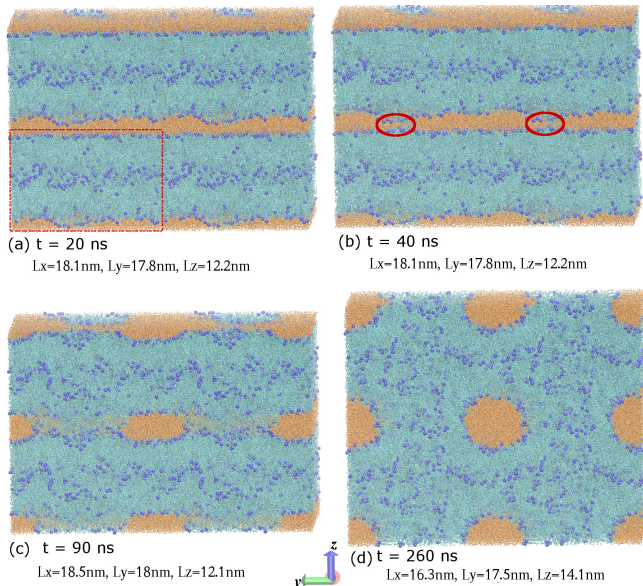


FIG. 4. SC lipid (cyan) double bilayer (equimolar CER, CHOL and FFA) with a thin layer of water (orange). There are no water molecules between the two bilayers. Nitrogen atoms in the head groups are shown as blue spheres. The simulation box is repeated once in both the y and z directions (The actual box dimension is indicated by dashed rectangle). (a): Lipid head groups in a small region across the thin water layer come closer to each other by natural fluctuations at around 20 ns. (b) The strong interaction between head groups pulls the leaflets closer (circled). (c) The water molecules evolve towards a cylindrical shaped region. Substantial rearrangement leads to a bilayer corona of lipid molecules around the water cylinder. (d) The structure remains stable for the rest of the simulation (260 ns) [35].

To further probe whether or not the inverse micellar phase is due to the preparation process, we created a dry double bilayer (1:1:1 composition). After equilibration with a continuous water wall along the z -direction, the continuous water wall was replaced by a thin layer of water (~ 1 nm) and standard periodic boundary conditions were used in all three directions. When, by natural fluctuation, a few of the lipid molecules in the outer leaflet of the top bilayer come in contact with the outer leaflet of the bottom bilayer across the thin water layer (via periodic boundary conditions), the head-head con-

tact area increases irreversibly, creating columns of water separated by the lipid corona (Fig. 4). The lipids retain a bilayer topology, with a cylindrical water column surrounded by *bilayers* instead of the usual monolayers.

A small fully hydrated bilayer of SC lipids is indefinitely stable in simulations. The local stress tensor across such a bilayer contains information about the spontaneous curvature favoured by the molecules [41]. Using local pressure tensor data from a 2:2:1 bilayer simulation, we find the spontaneous curvature c_0 for (half of) the bilayer as $1/c_0 \sim -15$ nm [35]. The sign of the curvature points towards equilibrium inverse phases and the magnitude is similar to the length-scale of the observed checkerboard pattern at the SC-SG boundary in cryo-EM [7].

Imposed layering near corneocyte: The corneocytes are surrounded by an envelope of grafted ceramide molecules whose fatty acid end is believed to be covalently bonded to the protein network in the corneocyte [42] (Fig. 1a). The highly hygroscopic corneocyte interior retains most of the water in the SC [40], leaving an essentially dry lipid matrix confined in the narrow space between corneocytes. The grafted ceramides in the corneocyte-bound lipid envelope (CLE) presents a patterned surface of favourable hydrogen-bond (H-bond) sites to this confined lipid matrix. By analogy with confined liquid crystals [43] and growth of colloidal crystals over patterned substrates [44], we expect that a surface with such patterning of favourable H-bonding sites will impose layering in the lipids. We model the CLE as a wall of hypothetical molecules formed by joining the two tails of a symmetric CER NS molecule with the mirror image of its head group (Fig. 5b). By construction, this molecule (termed CRW for corneocyte wall) forms a stable flat layer structure.

To be far from lamellar structure, we chose a final inverse-micellar phase configuration (2:2:1 lipid composition) as the starting point of this simulation. We partition the lipids along the z -direction by freezing the water molecules in a narrow strip, making that region unfavourable for the lipid molecules [35]. The structure away from this frozen water layer remain broadly unchanged. Next we slowly remove the water molecules, and equilibrate the lipids for 100ns between two continuous water walls. No layering developed during these steps (Fig. 5a). A layer of CRW was separately equilibrated with the number of CRW chosen to match the lateral dimension of the lipid system. The lipids were placed between the CRW walls. Fig. 5c shows the final configuration after subsequent evolution at 340K for 1μ s in the presence of the CRW wall. The lipid tails predominantly align perpendicular to the wall. Close to the wall, layering is near perfect and is parallel to the CRW walls. The ordering grows slowly due to low mobility of the molecules.

Discussion: These simulations show that the SC lipids form inverted micellar phases. A patterned wall mimicking the corneocyte-bound lipid envelope induces

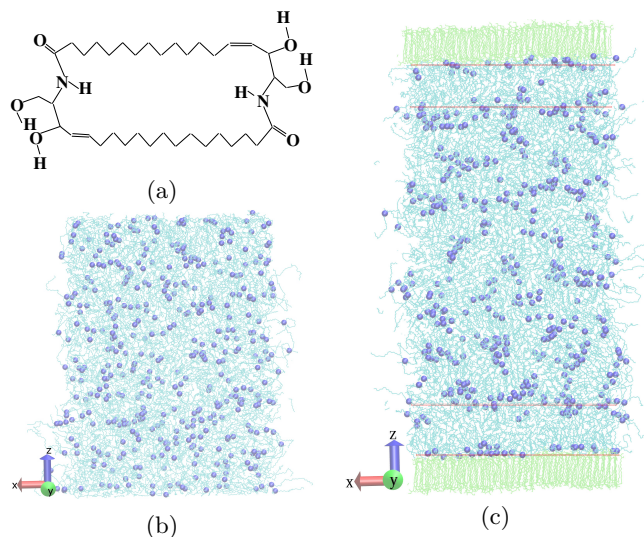


FIG. 5. (a) Schematic representation of hypothetical CRW molecule used to mimic corneocyte wall. (b) Configuration of lipids (cyan) with continuous wall (not shown) along the z -directions. Nitrogen atoms in the head groups are shown as blue spheres. The box size is $15.4\text{nm} \times 13.6\text{nm} \times 21.7\text{nm}$. (c) Configuration of lipids with CLE-mimic wall (lime) constructed with CRW molecules show layering, in contrast to continuous wall simulations. The two bilayers closest to the two walls are indicated by drawn lines. The box size is $13.6\text{nm} \times 12.3\text{nm} \times 28.8\text{nm}$. Only 3 nm slices along the y -direction are shown in (b) and (c).

layering in SC lipids. A continuous wall failed to induce layering, suggesting that the hydrogen-bonding with the wall molecules plays an important role in forming multi-layered structures.

These simulations provide some rationale behind the synthesis pathway and the lipid structures found in the SC *in vivo*. The seemingly unnecessary step of adding and removing a sugar group [23] becomes meaningful by noting that the ceramide lipids would have formed an inverse micellar phase if left without a large head group

inside the cells in the SG, and thus frustrate the vesicle trafficking mechanism necessary for their release. Once the sugar group is removed, if the molecules remain in the water-rich SG-SC boundary region they can form an inverse micellar phase, leading to the granular pattern seen in cryo-EM [7]. These water-containing inverted structures may play a role in the activity of anti-microbial peptides that are released along with the lipid molecules [22] and possibly are responsible for higher permeability in skin regions lacking corneocyte stacks [45]. Such non-lamellar structures have also been observed in some *in vitro* depositions [46]. When transported into the region between corneocyte walls, the patterned surface and confinement leads to a lamellar structure. The growth of this lamellar structure is necessarily slow because of low molecular mobility in the crowded confined environment. From *in vivo* measurement of recovery of permeability barrier, we expect the time-scale of this patterned wall induced ordering to be of order days [27] and the rate limiting step in the recovery process. The polydispersity stops the lipids from forming crystalline structures, thus providing some plasticity and dissipation. The polydisperse tails also lower the defect energies (as evidenced by the diffuse defect structure in fig. 4d) so that the lipids can envelope the corneocytes in three dimensions without forming strongly localised defects and thereby compromising the barrier.

ACKNOWLEDGMENTS

This work was supported by Yorkshire Forward through the grant YFRID Award B/302 and part financed by the European Regional Development Fund (ERDF). Computational resources were provided by SoftComp EU Network of Excellence. We gratefully acknowledge helpful comments by Patrick Warren. CD thanks Lars Nörlén for useful discussions and for sharing unpublished results.

-
- [1] P. M. Elias, *J. Invest. Dermatol.* **125**, 183 (2005).
 [2] M. R. Prausnitz, S. Mitragotri, and R. Langer, *Nat. Rev. Drug Discovery* **3**, 115 (2004).
 [3] A. S. Michaels, S. K. Chandrasekaran, and J. E. Shaw, *AICHE J.* **21**, 985 (1975).
 [4] A. Breathnach, T. Goodman, C. Stolinsky, and M. Gross, *J. Anat.* **114**, 65 (1973).
 [5] S. White, D. Mirejovsky, and G. King, *Biochemistry* **27**, 3725 (1988).
 [6] J. Boustra, G. Gooris, J. van der Spek, and W. Bras, *J. Invest. Derm.* **97**, 1005 (1991).
 [7] A. Al-Amoudi, J. Dubochet, and L. Nörlén, *J. Invest. Derm.* **124**, 764 (2005).
 [8] D. Groen, G. Gooris, M. Ponec, and J. Bouwstra, *BBA-Biomembranes* **1778**, 2421 (2008).
 [9] A. Schröter, D. Kessner, M. Kiselev, T. Hauß, S. Dante, and R. H. Neubert, *Biophys. J.* **97**, 1104 (2009).
 [10] L. Nörlén, *J. Invest. Derm.* **117**, 830 (2001).
 [11] D. Bommannan, R. O. Potts, and R. H. Guy, *J. Invest. Derm.* **95**, 403 (1990).
 [12] G. S. Pilgram, A. M. Engelsma-van Pelt, J. A. Bouwstra, and H. K. Koerten, *J. Invest. Derm.* **113**, 403 (1999).
 [13] D. C. Swartzendruber, P. W. Wertz, D. J. Kitko, K. C. Madison, and D. T. Downing, *J. Invest. Derm.* **92**, 251 (1989).
 [14] J. Bouwstra, G. Gooris, F. Dubbelaar, A. Weerheim, A. IJzerman, and M. Ponec, *J. Lipid Res.* **39**, 186 (1998).
 [15] B. Forslind, *Acta Dermatol. Venerol.* **74**, 1 (1994).
 [16] J. Hill and P. Wertz, *Biochim. Biophys. Acta - Biomembranes* **1616**, 121 (2003).
 [17] T. J. McIntosh, *Biophys. J.* **85**, 1675 (2003).
 [18] I. Iwai, H. Han, L. den Hollander, S. Svensson,

- L. Öfverstedt, J. Anwar, J. Brewer, M. Bloksgaard, A. Laloef, D. Nosek, S. Masich, L. Bagatolli, U. Skoglund, and L. Norlén, *J. Invest. Derm.* **132**, 2215 (2012).
- [19] L. Norlén, I. Nicander, B. L. Rozell, S. Ollmar, and B. Forslind, *J. Invest. Derm.* **112**, 72 (1999).
- [20] M. Bartek, J. Labudde, and H. Maibach, *J. Invest. Derm.* **58**, 114 (1972).
- [21] K. S. Wu, W. W. van Osdol, and R. H. Dauskardt, *Biomaterials* **27**, 785 (2006).
- [22] K. Aberg, M.-Q. Man, R. Gallo, T. Ganz, D. Crumrine, B. Brown, E.-H. Choi, D.-K. Kim, J. Schröder, K. Feingold, and P. Elias, *J. Invest. Derm.* **128**, 917 (2007).
- [23] Y. Mizutani, S. Mitsutake, K. Tsuji, A. Kihara, and Y. Igarashi, *Biochimie* **91**, 784 (2009).
- [24] A. Weerheim and M. Ponc, *Arch. Derm. Res.* **293**, 191 (2001).
- [25] H. Farwanah, J. Wohrab, R. H. H. Neubert, and K. Raith, *Anal. Bioanal. Chem.* **383**, 632 (2005).
- [26] G. K. Menon, K. R. Feingold, and P. M. Elias, *J. Invest. Derm.* **98**, 279 (1992).
- [27] G. Grubauer, P. Elias, and K. Feingold, *J. Lipid Res.* **30**, 323 (1989).
- [28] M. Höltje, T. Förster, B. Brandt, T. Engels, W. von Rybinski, and H.-D. Höltje, *Biochim. Biophys. Acta* **1511**, 156 (2001).
- [29] S. A. Pandit and H. L. Scott, *J. Chem. Phys.* **124**, 014708 (2006).
- [30] R. Notman, W. K. den Otter, M. G. Noro, W. J. Briels, and J. Anwar, *Biophys. J.* **93**, 2056 (2007).
- [31] C. Das, M. G. Noro, and P. D. Olmsted, *Biophys. J.* **97**, 1941 (2009).
- [32] C. Das, P. D. Olmsted, and M. G. Noro, *SoftMatter* **5**, 4549 (2010).
- [33] M. I. Hoopes, M. G. Noro, M. L. Longo, and R. Faller, *J. Phys. Chem. B* **115**, 3164 (2011).
- [34] T. Engelbrecht, T. Hauß, K. Süß, A. Vogel, M. Roark, S. Feller, R. Neubert, and B. Dobner, *Soft Matter* **7**, 8998 (2011).
- [35] Supplementary online material contains an introduction to the skin lipids, simulation details, and additional results. Animations of the trajectories of Fig. 3 and Fig. 4 are at <http://goo.gl/qqMzrE>.
- [36] H. J. C. Berendsen, D. van der Spoel, and R. van Drunen, *Comp. Phys. Comm.* **91**, 43 (1995).
- [37] S. Chiu, M. Clark, V. Balaji, S. Subramaniam, H. Scott, and E. Jakobsson, *Biophys. J.* **69**, 1230 (1995).
- [38] O. Berger, O. Edholm, and F. Jähnig, *Biophys. J.* **72**, 2002 (1997).
- [39] R. Warner, M. Myers, and D. Taylor, *J. Invest. Dermatol.* **90**, 218 (1988).
- [40] J. A. Bouwstra, A. de Graaff, G. S. Gooris, J. Nijse, J. W. Wiechers, and A. C. van Aelst, *J. Invest. Derm.* **120**, 750 (2003).
- [41] J. M. Seddon, *Biochim. Biophys. Acta* **1031**, 1 (1990).
- [42] D. Swartzendruber, P. Wertz, K. Madison, and D. Downing, *J. Invest. Derm.* **88**, 709 (1987).
- [43] A. Ajdari, L. Peliti, and J. Prost, *Phys. Rev. Lett.* **66**, 1481 (1991).
- [44] J. P. Hoogenboom, A. K. van Langen-Suurling, J. Romijn, and A. van Blaaderen, *Phys. Rev. Lett.* **90**, 138301 (2003).
- [45] A. Schätzlein and G. Cevc, *British Journal of Dermatology* **138**, 583 (1998).
- [46] I. Plasencia, L. Norlén, and L. A. Bagatolli, *Biophys. J.* **93**, 3142 (2007).

Supplementary material:

Lamellar and inverse micellar structures of skin lipids:
Effect of templating

Chinmay Das, Massimo G. Noro and Peter D. Olmsted

S1. STRATUM CORNEUM LIPID MOLECULES

Epidermis, the outer layer of the skin, has a stratified organization and is named according to the visual appearance under optical microscope (Fig. S1.a). The *stratum corneum* (SC) is the outermost layer of the epidermis, comprising dead pancake-like flattened cells (corneocytes) in a lipid matrix. Keratinocytes, the dominant cell type in the *stratum basale*, the innermost layer of epidermis, migrate through the intervening layers while changing in shape and content. In the *stratum granulosum*, immediately below the SC, keratinocytes over-produce keratin and secrete specialized lipids. By the time keratinocytes migrate to SC, the nuclei and other internal organelles disintegrate and the cell attains a comparatively rigid structure through keratin network. The dead keratinocytes are called corneocytes. The lipid matrix in the SC provides the main barrier against water loss and invasion of foreign pathogens [1].

The lipid matrix in the extracellular space of the corneocytes shows a multilamellar structure in electron microscopy (Fig. S1.b) [2]. This multilamellar structure is often punctuated by *lacunar spaces* where the periodic structure in electron density is lost. The lipids adjacent to the corneocytes are covalently bound to the protein network of the corneocytes forming the *corneocyte-bound lipid envelope* (CLE) (Fig. S1.c), which shows up as electron-dense regions in electron microscopy.

The main components of the SC lipid matrix are the ceramide sphingolipids (CER), cholesterol (CHOL) and free fatty acid (FFA). There are 11 families of CER molecules found in the SC (Fig. S2), differing by the numbers and the positions of the hydroxyl groups. Each member of these CER families shows additional polydispersity in the number of carbons in the fatty acid tail motif, leading to more than 300 different CER molecules [6]. We refer to the molecules by their family names followed by the number of carbon atoms in the fatty acid motif. Thus, CER NS 24 refers to CER NS with lignoceric acid as the fatty acid motif. Similarly the different FFA molecules are distinguished by the number of carbon atoms. In the literature, ceramide families often are distinguished by the order of their appearance in the chromatograph: CER EOS is often referred to as ceramide 1, CER NS as ceramide 2 and CER NP as ceramide 3.

S2. SIMULATION DETAILS

All simulations were carried out with the molecular dynamics software GROMACS [7,8] with Nosé-Hoover ther-

mostats separately coupled to the lipid molecules and the water molecules, and with a Parrinello-Rahman barostat. Bond lengths were constrained with the LINCS algorithm for the lipid molecules and with the SETTLE algorithm for water molecules. The time steps for MD simulations were 2 fs.

We used the ‘Berger’ force-field [9] for the lipid molecules, which accurately reproduces experimental results for different lipid systems [10]. We have used the same force-field in the past for simulations of a smaller subset of SC lipid molecules for studying small fully hydrated bilayers and water permeation [11,12]. Water is modeled with the SPC potential [13]. The partial charges used are shown in Fig.S3.

We use a group-based cut-off with the cut-off length 1.2 nm for both the van der Waals and electrostatic interactions. In our previous simulations [11], we have explicitly compared simulations involving a group-based cut-off with particle-mesh Ewald summation (PME) simulations. The effect of the long range electrostatics was found to be negligible. In simulations of lipid bilayers, long range electrostatics often plays an important role. The reasons for the negligible contribution of long range electrostatics in our simulations are two-fold: Firstly, the SC lipids are uncharged at skin pH, with only small partial charges contributing to the electrostatic interaction. Thus, the dipole moments involved are about 15 times smaller than the typical phospholipid dipole created from well separated N^- and P^+ charges. Secondly phospholipid dipoles have a component normal to the water-lipid interface, which can give rise to a macroscopic dipole moment. By contrast, the small dipoles from the partial charges in the SC lipid system, even in a bilayer arrangement, orient themselves in random directions. Thus, the effect of the electrostatic interaction beyond the cut-off becomes much smaller than the thermal energy.

Table S1 gives the number of molecules used in the different simulations. Guided by the mass-spectroscopic profiles for the ceramides [14,15], we choose a fixed molar ratio 1:5:4 for the CER EOS : CER NS : CER NP. In doing so, we assume that the ceramides with esterified ω -hydroxy fatty acids (CER EOS, CER EOH and CER EOP) behave similarly and CER EOS alone represents all three of these families in our simulations. Similarly, ceramides that do not have such esterified fatty acid and have a double bond in the sphingosine motif are represented by CER NS. CER NP accounts for rest of the ceramides (all of which do not have double bonds in the sphingosine motif). Set A and set C consider CER, CHOL and FFA in 1:1:1 molar ratio. Set B considers a molar ratio of CER : CHOL : FFA = 2:2:1. Set A and set B contains 30 wt% water. In both of these two sets (A and B), three separate simulations were performed with different initial conditions, which we will distinguish as set Aa, set Ab and so on. Set C was used to look at the stability of pre-formed multilayer arrangements (Details follow in S2.4).

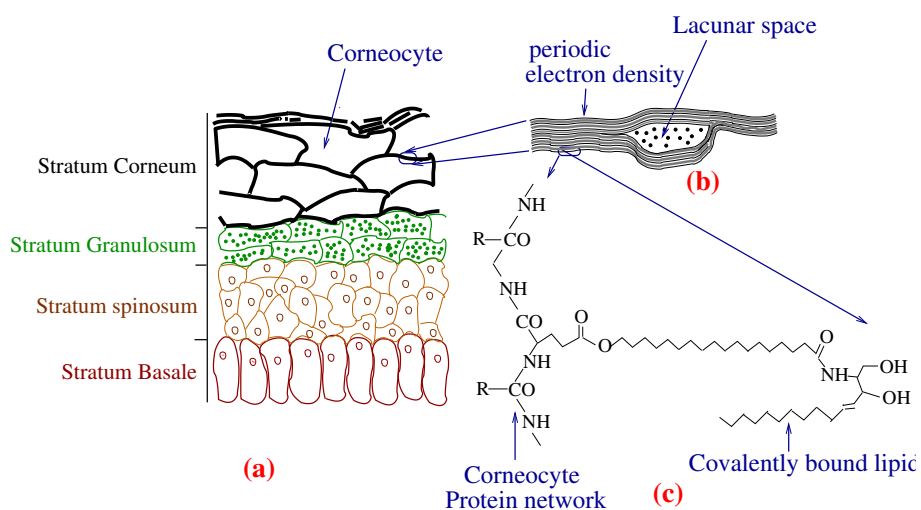


FIG. S1. (a) Schematic representation of the layers in the epidermis. (b) The inter-corneocyte region is filled with specialized lipids whose electron density shows a multilamellar structure. The lamellar regions are punctuated by *lacunar spaces* (schematic figure based on [2,3]). (c) Some of the lipids are covalently bound to the protein networks in the corneocytes (schematic figure based on [4]).

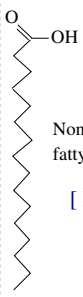
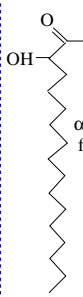

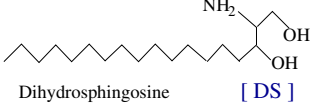
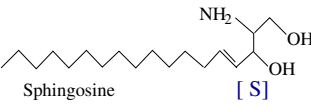
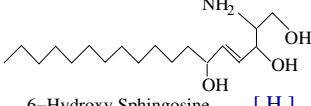
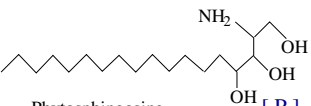
Fatty acid motif			
Sphingosine motif	[N]	[A]	[EO]
 Dihydrosphingosine [DS]	CER-NDS	CER-ADS	---
 Sphingosine [S]	CER-NS (CER2)	CER-AS (CER5)	CER-EOS (CER1)
 6-Hydroxy Sphingosine [H]	CER-NH (CER8)	CER-AH (CER7)	CER-EOH (CER4)
 Phytosphingosine [P]	CER-NP (CER3)	CER-AP (CER6)	CER-EOP (CER9)

FIG. S2. Ceramide family in the SC lipid matrix. Each of the members consists of a sphingosine motif bonded via a peptide (amide) bond to a fatty acid motif. The fatty acid motif shown here is palmitic acid (16 carbon). Ceramides in the SC contain variable length fatty acids (typically 20 to 30 carbon atom long). (Adapted from [5])

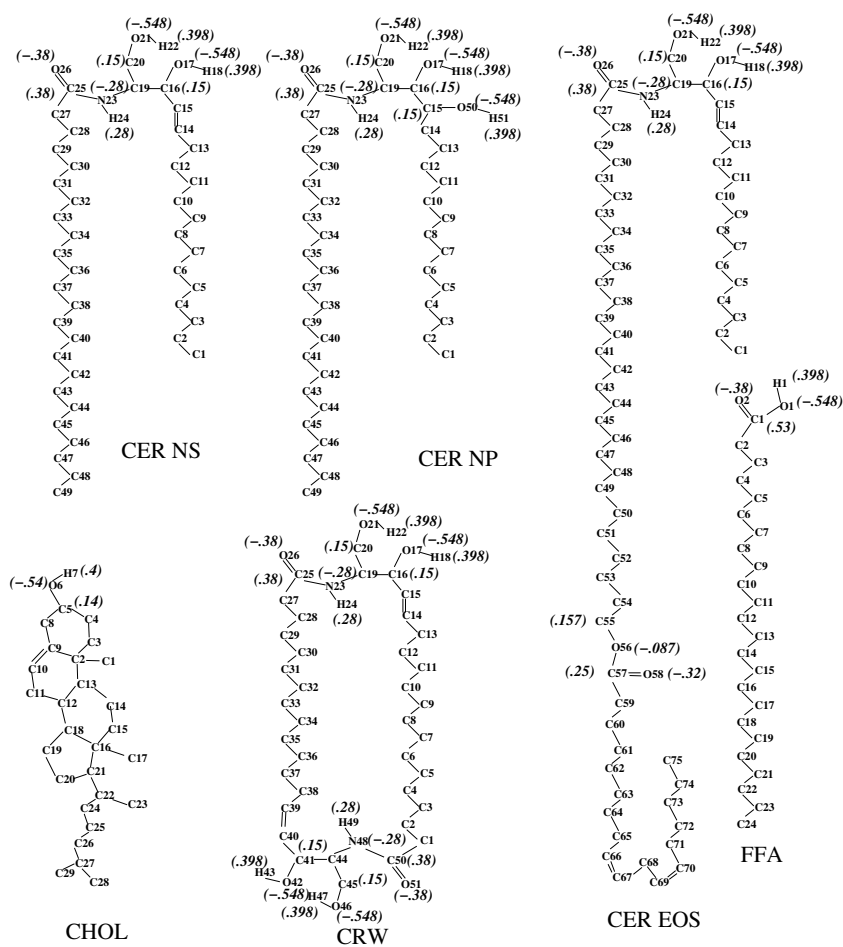


FIG. S3. Partial charges used for the different lipid molecules.

molecule family	fatty acid tail (number of carbons)	Number of molecules		
		setA	set B	set C
CER EOS	30	30	30	20
	32	80	80	52
	33	30	30	20
	34	60	60	40
CER NS	22	100	100	68
	24	200	200	132
	25	100	100	68
	26	300	300	200
	28	200	200	132
CER NP	24	80	80	52
	26	136	136	92
	28	208	208	140
	30	240	240	160
	32	136	136	92
FFA	20	100	50	64
	22	200	100	136
	24	800	400	536
	25	200	100	136
	26	460	230	304
	28	200	100	136
30	40	20	24	
CHOL	–	2000	2000	1332
SOL	–	50000	43600	20000
Molar ratio CER:CHOL:FFA		1:1:1	2:2:1	1:1:1

TABLE S1. Numbers of molecules used in the simulations. For the sets A and B, we use three different initial configurations. The three configurations from set A are referred to as sets Aa, Ab and Ac. A similar suffix is used for set B.

S2.1. Inverse micellar phase

Configurations with a single molecule of each of the lipid species were energy minimized in vacuum separately. For the simulations in sets A and B, a large simulation box was divided into small grids with dimensions large enough to accommodate the longest lipid species. The desired number of energy-minimized lipid molecules were placed with random orientations in randomly selected unoccupied grid points. We maintain a finer grid which notes occupied sites by individual lipid atoms. The required number of water molecules were placed with random orientations at randomly chosen unoccupied sites of the fine grid.

The configurations were energy minimized and evolved with NPT MD steps using a Nose-Hoover thermostat and a Parrinello-Rahman barostat for 50 ns at 340 K. Standard periodic boundary conditions in a cubic simulation box and isotropic pressure coupling were used in all cases except for set Bc.

For one of the 2:2:1 composition system (set Bc), we selected a rectangular box with x - y dimensions nearly four times larger than the z direction ($L_x = L_y = 175$ nm, $L_z = 56$ nm). Once the initial ‘gas’-phase system reached

atmospheric pressure, an anisotropic barostat with a large (1000 bar) pressure applied along the $x - y$ directions and atmospheric pressure applied in the z direction was used to achieve a nearly cubic box. The resulting deformation aligns the long molecules preferentially along the z direction. After this, the pressure couplings were set to atmospheric pressure in all three directions and the system was evolved for 50 ns at 340 K. The initial alignment did not affect the transition to the final inverse micellar arrangement with on average isotropic lipid orientations. We evolved this set Bc for a further 50 ns at an elevated temperature of 350 K and then finally for another 100 ns at 300 K. The inverse micellar arrangement was found to be robust under change in temperature. The final configurations of the different sets are presented in Fig. S4 and Fig. S5.

S2.2. Surface-templated lipid system

In the final inverse micellar configuration of set Bc we selected a 1 nm zone, within which the water molecules were frozen along the z -direction. We repeatedly carried out short (1 ps) NVT simulations and identified any new water molecules drifting in the selected zone. These water molecules in turn were added to the frozen list. Locally this creates enough perturbation to move the lipid molecules out of this zone. Only a few lipid tails stay stuck in the frozen water layer. They were pulled out of the water layer by moving them at a constant speed (0.01 nm/ps) away from the water layer. The configuration created by this process is shown in Fig. S6 a. The inverse micellar structure away from the frozen water layer remain unchanged during further evolution (50 ns, Fig. S6 b).

The frozen water layer allows us to introduce a wall along the z -direction mimicking a continuous distribution of water molecules. The walls interact with the atoms as an integrated Lennard-Jones (9-3) potential with interaction parameters chosen to be that of atom type OW (oxygen of water) at density 33.44 atoms/nm³. After 50 ns of NPT simulation, no qualitative change in the lipid arrangement was observed (Fig. S6 b).

In SC, the lipids between highly hygroscopic corneocytes are essentially free of water [16]. To simulate at conditions similar to that between corneocytes, we *dry* the lipid structure by slowly removing the inner water molecules (10 randomly water molecules were removed every 100 ps of NPT simulation), and evolve the system for another 50 ns with a continuous water wall. The anisotropy introduced by the walls along the z -direction changes the box dimension significantly (Fig. 4a). But no signature of layering was observed. Specifically, the hydrocarbon tails were found to be equally likely to be parallel to the wall as perpendicular to the wall for lipids close to the boundaries.

In the SC, a layer of ceramide molecules are covalently bonded to the proteins in corneocyte. Thus the CLE

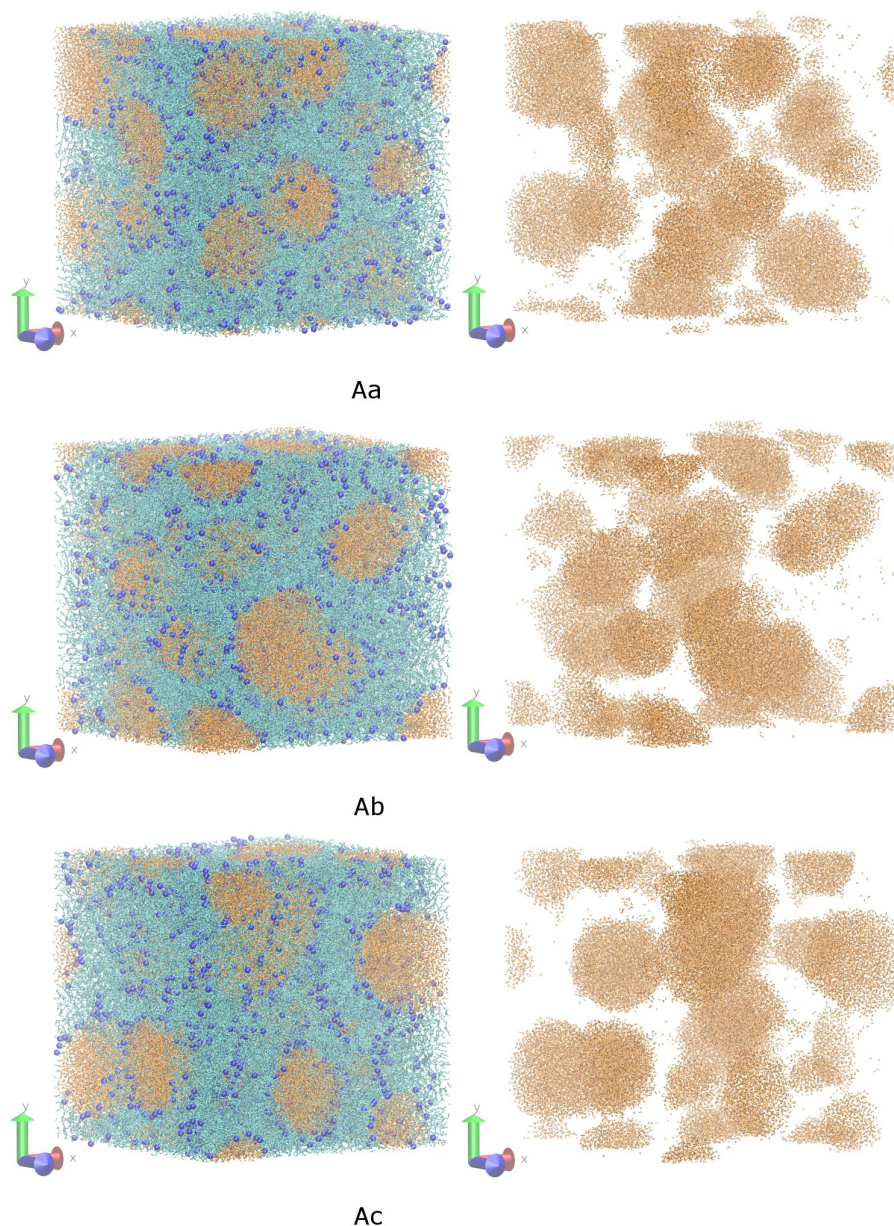


FIG. S4. Final configurations of the three simulations with 1:1:1 molar concentration of CER, CHOL and FFA (Sets Aa, Ab and Ac). The right-hand panel shows only the water molecules to highlight the disconnected water clusters. The box dimension is ~ 18.8 nm in all three configurations.

surface presents itself as a well aligned layer of ceramide head groups to the stratum corneum lipids. In our next step we try to mimic this surface.

First we replace the continuous wall with a layer of SPC water molecules (24000 molecules) and use 100 ns of NPT simulation. Discrete water molecules provide transient hydrogen bonds that align the lipids closest to the boundary, and the lipid tails align predominantly along the z -direction (Fig. S7). From a separate simulation of a hydrated bilayer comprising CER NS 24:0, a single molecule with a hairpin conformation was isolated. The

head group (atoms between C16 till O26) was duplicated (as atoms C41 till O51). The new copy of the head group was mirrored first about z -axis and then about the nitrogen atom. Finally the new group was given a rigid translation by identifying the terminal CH3 group of the fatty acid chain of original molecule as C41 of the duplicated head group. We term this artificial lipid molecule CRW. Because of the symmetry of this molecule, it has zero curvature and a flat layer structure will be its preferred arrangement. All interaction parameters of the new second head group are identical to the first head group. The

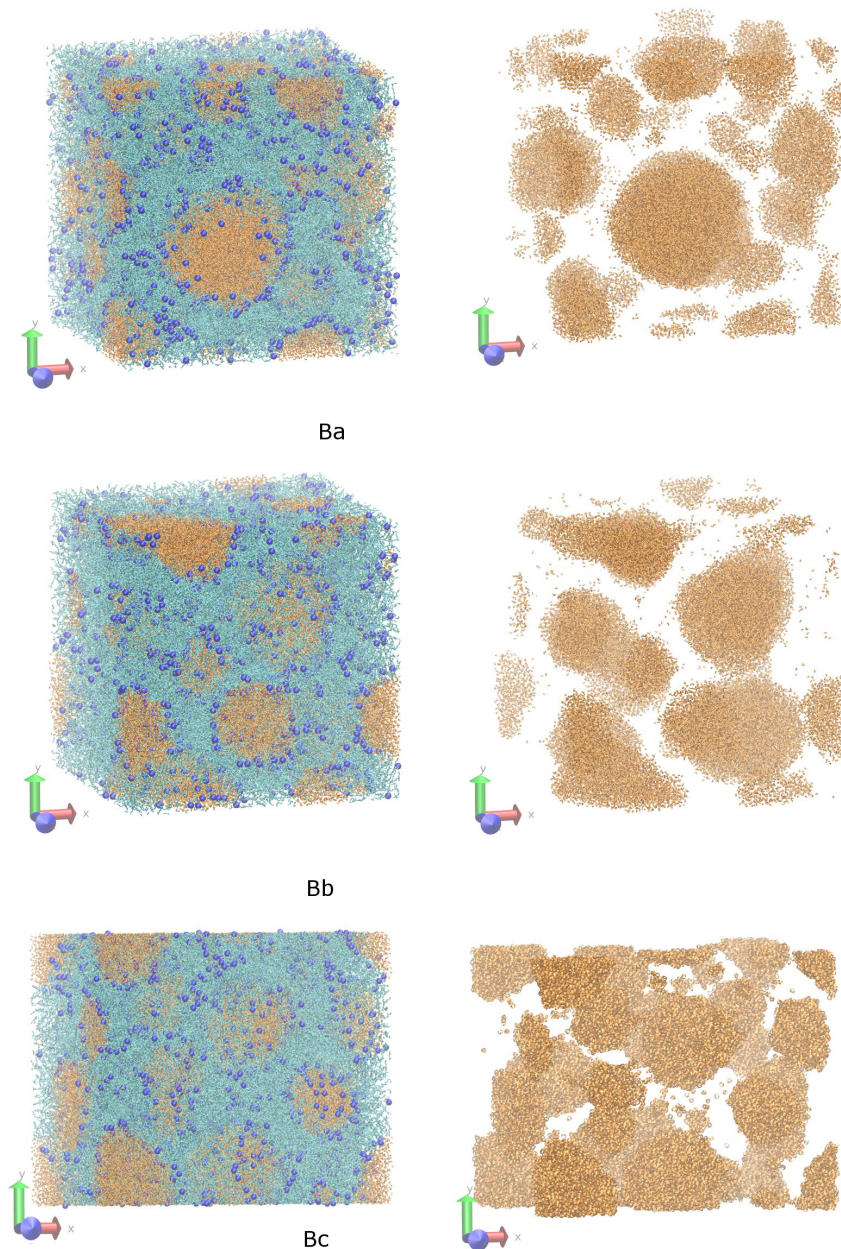


FIG. S5. Final configurations of the three simulations with 2:2:1 molar concentration of CER, CHOL and FFA. The right-hand panel shows only the water molecules to highlight the disconnected water clusters. Sets Ba and Bb are 50 ns after density equilibration. Set Bc is evolved for a further 50 ns at 340K and another 100 ns at 300K. Sets Ba and Bb are in cubic box with dimension ~ 17.9 nm. The box size for set Bc is $20.3 \text{ nm} \times 17.1 \text{ nm} \times 16.2 \text{ nm}$.

molecule was placed in vacuum and energy minimized.

The existing lipid box in which we wanted to include the CRW wall had $x - y$ box dimensions of $13.37 \text{ nm} \times 12.10 \text{ nm}$. Guided by the area/lipid of CER 2 bilayers [11], we placed 408 CRW molecules in a roughly triangular lattice with the $x - y$ dimensions of the box identical to the SC lipid system. We place two continuous water walls along the z -direction at separation of 3.8 nm . The molecules were energy minimized, and then equilibrated over 0.5 ns with NVT MD simulations at 340K .

This equilibrated CLW layer was included in place of the water wall in the SC lipid box. The configuration was energy minimized and evolved for further $1 \mu\text{s}$ at 340 K with NPT simulation. The final configuration of this system is shown in the main body of the paper (Fig. 4c). Close to the two walls, the figure shows aligned bilayers. Further away from the walls, patches of bilayer can be seen that are not oriented with the wall. The long timescale of realignment of the interior bilayer patches may explain the long delay between the lipid release from

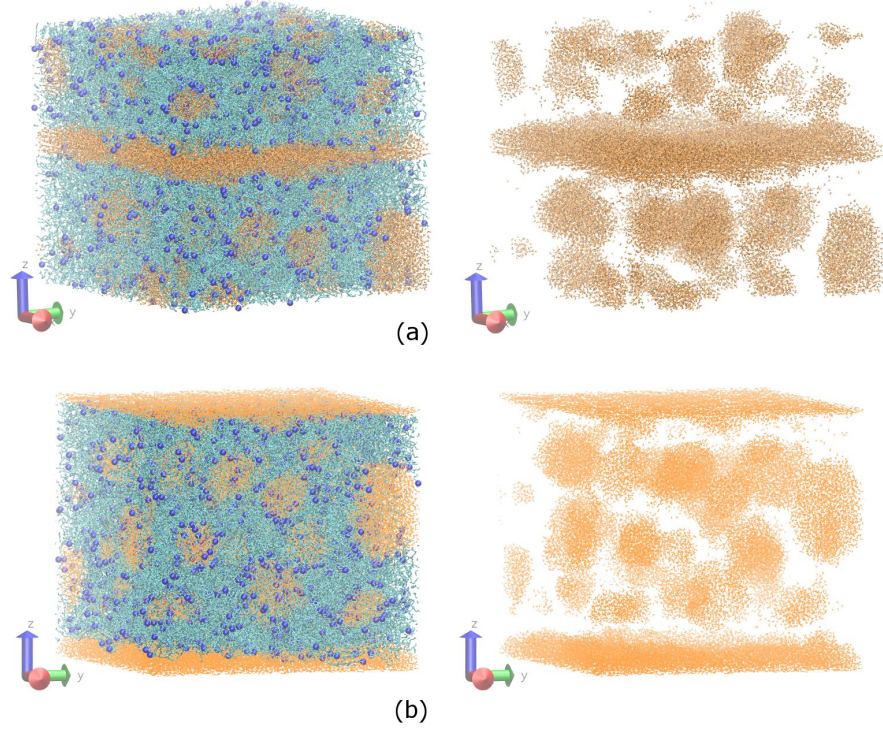


FIG. S6. (a) Simulation of set Bc with water molecules frozen in 1 nm region at the center of the box. Box size is $19.5 \text{ nm} \times 17.4 \text{ nm} \times 16.3 \text{ nm}$. (b) The procedure allows us to introduce a wall keeping the inverse micellar arrangement. The box size is $19.5 \text{ nm} \times 17.4 \text{ nm} \times 16.7 \text{ nm}$.

SG and recovery of the permeability barrier.

S2.3. Signature of inverse micellar phase in hydrated bilayer

CER NS tails are identical to sphingomyelin (SM) except for the absence of the phosphocholine head group. The absence of the phosphocholine headgroup leads to an area/lipid [11] that is only around 70% of that for SM in a hydrated bilayer [17]. Since SM forms a stable bilayer, from geometric consideration alone [18], one would expect CER to form an inverted phase. In fact, in all but one of the several crystal structures CER adopts a splayed chain arrangement [19] to release the packing frustration of accommodating a small head and comparatively bulky tails.

While a small bilayer with full hydration is indefinitely stable in simulations, the local stress tensor across the bilayer contains information about the spontaneous curvature preferred by the molecules. The integral of the first moment of the difference in the lateral (P_{LAT}) and the normal pressure (P_{zz}) profile is related to the spontaneous curvature c_0 and the bending elastic constant κ

for (half of) the bilayer through [20]

$$\kappa c_0 = 2 \int z [P_{LAT}(z) - P_{zz}(z)] dz. \quad (\text{S1})$$

Here, $P_{LAT} \equiv \frac{1}{2} [P_{xx} + P_{yy}]$ and the integral is assumed to be over a single monolayer. In the literature, this expression is often written in terms of tension, which is the negative of the lateral pressure. Also, different prefactors are used for different definitions of the bending modulus.

Calculation of the local microscopic pressure tensor is costly and we have not attempted such calculations for these simulations. However, we have re-analyzed the result of a CER NS 24 hydrated bilayer and a 2:2:1 hydrated bilayer comprising CER NS 24, FFA 24 and CHOL from [11]. In Fig S8 we show the lateral pressure profiles at 340K after smoothing the data by combining results from both the monolayers because of the up-down symmetry, and a further three point smoothing.

Using the bending modulus values from [11] (6.6×10^{-11} erg for the CER NS bilayer and 3.3×10^{-11} erg for the 2:2:1 bilayer), numerical integration of eq. S1 then gives $1/c_0 \sim -44 \text{ nm}$ for (half of) the CER NS bilayer and $1/c_0 \sim -15 \text{ nm}$ for (half of) the mixed lipid bilayer. The sign of the curvature points towards equilibrium inverse phases and the magnitude is similar to the length-scale of the observed checkerboard pattern in cryo-EM [2].

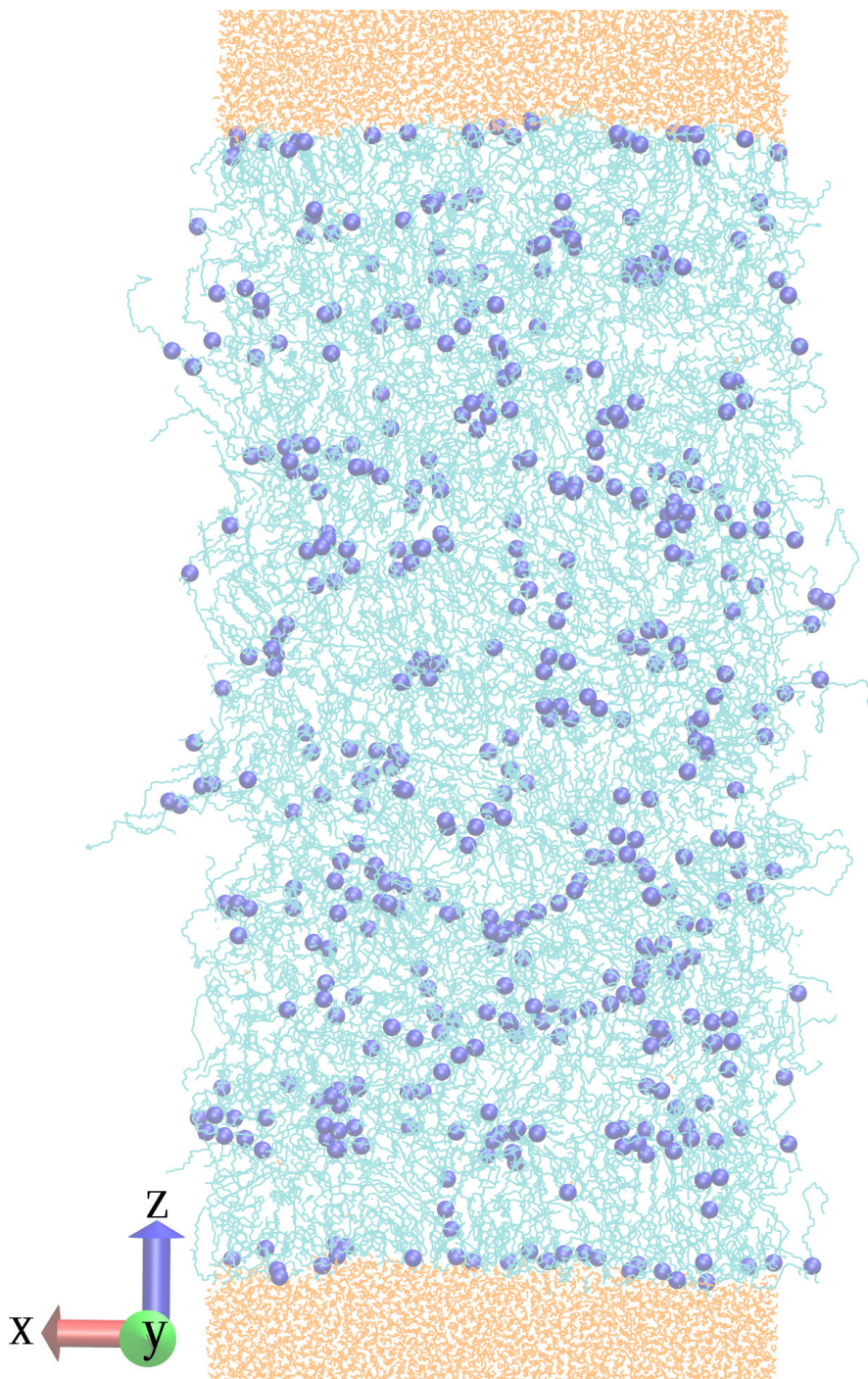


FIG. S7. Lipids from set Bc after evolving for 100 ns, placed between water walls along the z -direction. Box dimensions are $13.4 \text{ nm} \times 12.1 \text{ nm} \times 32.1 \text{ nm}$. Only a 3 nm slice along the y -direction is shown.

S2.4. Pre-formed multilayers

Separate leaflets with the same number of lipid molecules in each leaflet were prepared by randomly placing the lipid molecules with the CER tails in hairpin arrangements and with the head groups at the same z . Four such leaflets were energy minimized and joined to

form a double bilayer structure with sufficient separation between the leaflets to accommodate the longest lipid species without overlap with the adjacent leaflet. Continuous water wall was placed along the z -directions. The structure was repeatedly compressed in $x - y$ direction by 1%, the leaflets were moved closer to each other by 0.001 nm, and energy minimized. This ensures that the lipids remain in multilayer arrangement, while

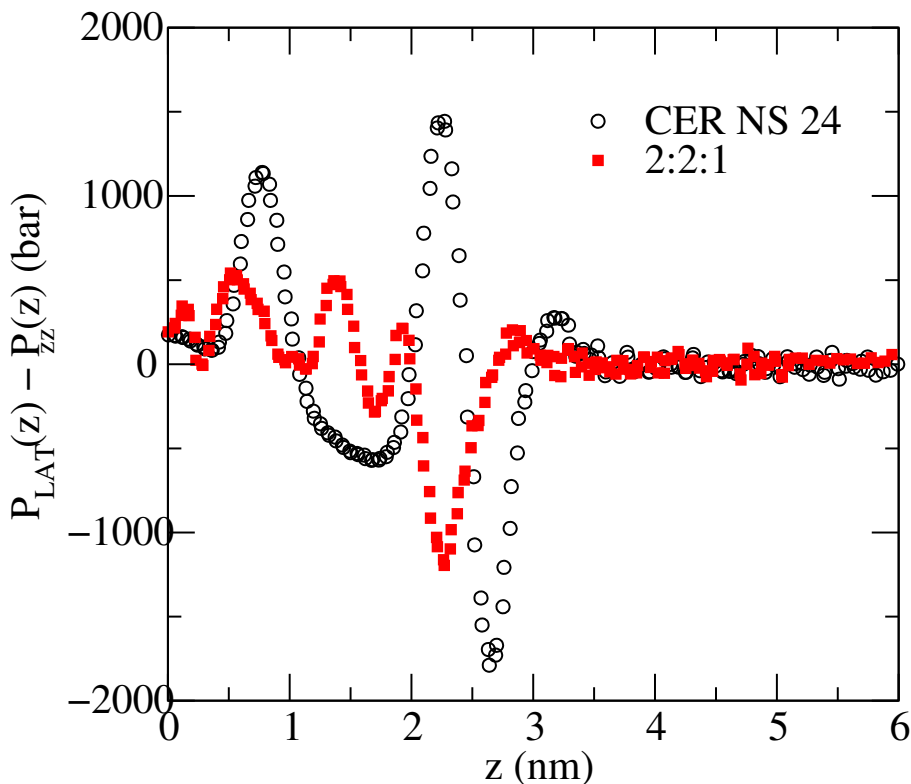


FIG. S8. Lateral pressure profile for CER NS 24 bilayer (open circles) and bilayers of CER NS 24, FFA 24 and CHOL at 2:2:1 molar ratio (squares). The distance z is measured from the bilayer center of mass and the data is averaged over both the monolayers. (Adapted from [11])

locally deforming to allow a liquid-like dense configuration. Once the internal pressure reached one atmosphere, a layer of water (20000 molecules, ~ 1 nm) was placed in place of the wall, and for 1 ns only the water molecules were evolved with NVT simulation while keeping the lipid molecules frozen. Finally the constraints were removed and NPT steps were used to further evolve the system for 260 ns. We also simulated multilayers with identical preparation steps except with a thicker water layer (25000 molecules). Multilayers remain stable for the entire simulation duration (260 ns) in such cases.

S2.5. Preparation of the simulation snapshots

The figures showing simulation snapshots were prepared with the package Visual Molecular Dynamics (VMD, www.ks.uiuc.edu/Research/vmd), rendered with Persistence of Vision Raytracer (POV-Ray, www.povray.org) and annotated with GNU image Manipulation Program (GIMP, www.gimp.org).

REFERENCES

- [1] Ruth K. Freinkel and David T. Woodley, eds. *The biology of the skin*. (Parthenon Publishing, London, 2001).
- [2] A. Al-Amoudi, J. Dubochet, and L. Norlén, *J. Invest. Derm.*, **124**, 764 (2005).
- [3] S. Paliwal, G.K. Menon, and S. Mitragotri, *J. Invest. Derm.*, **126**, 1095 (2006).
- [4] D.C. Swartzendruber, P.W. Wertz, K.C. Madison, and D.T. Downing, *J. Invest. Derm.*, **88**, 709 (1987).
- [5] J. Ishikawa, H. Narita, N. Kondo, M. Hotta, Y. Takagi, Y. Masukawa, T. Kitahara, Y. Takema, S. Koyano, S. Yamazaki, and A. Hatamochi, *J. Invest. Derm.*, **130**, 2511 (2010).
- [6] Y. Masukawa, H. Narita, H. Sato, A. Naoe, N. Kondo, Y. Sugai, T. Oba, R. Homma, J. Ishikawa, Y. Takagi, and T. Kitahara, *J. Lipid. Res.*, **50**, 1708 (2009).
- [7] D. van der Spoel, E. Lindahl, B. Hess, G. Groenhof, A. E. Mark, and H. J. C. Berendsen. Gromacs: Fast, flexible and free. *J. Comp. Chem.*, **26**, 1701 (2005).
- [8] D. van der Spoel, E. Lindahl, B. Hess, A. R. van Buuren, E. Apol, P. J. Meulenhoff, D.P. Tieleman, A. L.

- T. M. Sijbers, K. A. Feenstra, R. van Drunen, and H. J. C. Berendsen, *Gromacs User Manual version 3.3*. www.gromacs.org (2005).
- [9] S.W. Chiu, M. Clark, V. Balaji, S. Subramaniam, H.L. Scott, and E. Jacobsson, *Biophys. J.*, **69**, 1230 (1995).
- [10] O. Berger, O. Edholm, and F. Jähnig, *Biophys. J.*, **72**, 2002 (1997).
- [11] C. Das, M. Noro, and P. D. Olmsted, *Biophys. J.*, **97**, 1941 (2009).
- [13] C. Das, P. D. Olmsted, and M. G. Noro, *SoftMatter*, **5**, 4549 (2009).
- [14] A. Weerheim and M. Ponc, *Arch. Derm. Res.*, **293**, 191, (2001).
- [15] H. Farwanah, J. Wohlrab, R. H. H. Neubert, and K. Raith, *Anal. Bioanal. Chem.*, **383**, 632 (2005).
- [16] J. A. Bouwstra, A. de Graaff, G. S. Gooris, J. Nijse, J. W. Wiechers, and A. C. van Aelst, *J. Invest. Derm.*, **120**, 750 (2003).
- [17] E. Mombelli, R. Morris, W. Taylor, and F. Frater-nali, *Biophys. J.*, **84**, 1507 (2003).
- [18] J. N. Israelachvili, *Intermolecular and surface forces*. (Academic Press, London, 1991).
- [19] J. Shah, J. M. Atienza, R. I. Duclos Jr., A. V. Rawlings, Z. Dong, and G. G. Shipley, *J. Lipid Res.*, **36**, 1936 (1995).
- [20] J. M. Seddon, *Biochim. Biophys. Acta*, **1031**, 1 (1990).